

# Short baseline neutrino experiment in nuclear reactors in Argentina

Contribution to the Latin American Strategy Forum for Research Infrastructure

*Draft version*

**Thematic areas:** Neutrino Physics, Beyond Standard Model, Instrumentation and Computing

**Primary authors:** Guillermo Fernandez Moroni<sup>1</sup>, Dario Rodrigues F. Maltez<sup>2,3</sup>, Miguel Sofo Haro<sup>4</sup>, Carla Bonifazi<sup>5,6</sup>, Ivan Sidelnik<sup>3,4</sup>, Jeronimo Blostein<sup>3,4</sup>, Pedro Machado<sup>7</sup>, Gustavo Cancelo<sup>7</sup>, Fernando Chierchie<sup>1</sup>, Federico Izraelevitch<sup>3,8</sup>, Leandro Stefanazzi<sup>1</sup>

<sup>1</sup> Instituto de Investigaciones en Ingeniería Eléctrica "Alfredo Desages", Bahía Blanca, Argentina.

<sup>2</sup> Departamento de Física, UBA, Argentina

<sup>3</sup> Consejo Nacional de Investigaciones Científicas y Técnicas, Argentina.

<sup>4</sup> Instituto Balseiro - Centro Atómico Bariloche, UNCuyo-CNEA, Argentina.

<sup>5</sup> Instituto de Física - Universidade Federal do Rio de Janeiro, Brazil.

<sup>6</sup> International Center for Advanced Studies, UNSAM, Argentina.

<sup>7</sup> Fermilab, USA.

<sup>8</sup> Dan Beninson, UnSam, Argentina.

## Contact persons:

Dr. Guillermo Fernandez Moroni, email: gfmoroni@fnal.gov

Dr. Dario P. Rodrigues F. Maltez, email: rodriguesfm@df.uba.ar

Dr. Ivan Sidelnik, email: ivan.sidelnik@gmail.com

## Abstract

The neutrino community around the world is moving towards experiments in the low energy range, below the inverse beta decay process. The main reason for this is the large number of opportunities available in that range to study non-standard neutrinos interaction and physics beyond the standard model fields. Argentina has an excellent opportunity to take advantage of its experience in the nuclear field and in the development of low threshold detectors to develop a neutrino experiments using nuclear reactor as neutrino sources. Here, we propose the use of the new technologies called the Skipper-CCD, in a short baseline reactor neutrino experiment. We also discuss the benchmark models and we compare the reliability to observe the Coherent Neutrino Nucleus scattering in the most powerful reactors available in Argentina.

## List of the interested scientists in the community:

Juan Cruz Estrada Vigil, Fermilab, USA.  
Javier Tiffenberg, Fermilab, USA.  
Ricardo Piegaia, Departamento de Fisica, UBA-CONICET, Argentina.  
Gustavo Otero y Garzon, Departamento de Fisica, UBA-CONICET, Argentina.  
Xavier Bertou, Centro Atomico Bariloche, CNEA-CONICET, Argentina.  
Eduardo Paolini, IIIE, Bahia Blanca, Argentina.  
Daniel E. Lopez-Fogliani, IFIBA/DF, UBA-CONICET. Renata Zukanovich, USP, San Pablo, Brazil.  
Maximo Ave, USP, San Pablo, Brazil.  
Alexis Luszczak, FCEyN UBA, Argentina.  
Andres Daniel Perez, IFIBA-CONICET, Argentina.  
Belén Andrada, ITeDA, Argentina.  
Fernando Gollan, ITeDA, Argentina.  
Hernan Wahlberg, Universidad Nacional de La Plata - IFLP, Argentina.  
Ingo Allekotte, CNEA, Argentina.  
Julián Gasanego Barbuscio, Facultad de Ciencias Exactas y Naturales, UBA, Argentina.  
Karina Pierpauli, CNEA, Argentina.  
Leonardo Javier Galeta, Proyecto RA-10, CNEA, Argentina.  
Luis Horacio Arnaldi, CNEA-IB, Argentina.  
Maria Florencia Daneri, UBA, Argentina.  
Matias Hampel, ITeDA, Argentina.  
Pablo Armando Bellino, CNEA, Argentina.  
Paulina Knees, UBA, Argentina.  
Juan Carlos D'Olive, UNAM, Mexico.  
Jorge Molina, UNA, Paraguay.  
Martín Makler, CBPF, Brazil & ICAS-UNSAM, Argentina.  
Irina Nasteva, UFRJ, Brazil.  
Ben Kilminster, University of Zurich, Switzerland.

## Current status and expected challenges:

A group from people from the scientific community interested in this experiment is already organized and writing a technical report for summarizing its perspectives. In this context, a workshop was organized in December 17-19 at ICAS, UNSAM, Buenos Aires, Argentina. See the indico web page for further details, <https://indico.cern.ch/event/854531/>. Small prototypes are being built to evaluate the technological challenges for a big experiment. Also, this community has started communication with the institutions from two reactors in Argentina (one power reactor, one research reactor) to evaluate the possibilities of placing the prototype in their facilities.

## Construction and operational costs:

Item	Estimated cost /1000 USD	Notes
CCDs	600	300k per 240 CCDs
CCD package	20	1000 USD perCCD
Readout electronics	70	200 USD per channel
Cryogenics	20	-
Vacuum vessel	100	From electroformed copper
Shield	50	-
Other Components	25	IR shield, data acquisition
Total	885	-

Table 1: Preliminary estimate of the cost for 1 kg experiment.

## Computing requirements:

Taking into account the amount of data that will be generated by measurement of all detectors a huge store capacity of 100 Terabytes per year will be needed. The analysis of such an images also requires a large calculation capacity that could be covered by 10 last generation desktop computers or equivalent server equipment in parallel computation.

## 1 Scientific Context

The interest in explore the low neutrino energy is growing since new interactions, beyond the Standard Model, could exist between neutrinos and the matter. These could be mediated by electrically neutral particles yet to be discovered. If these particles are weakly coupled and sufficiently light, much below the weak scale, high energy experiments such as the LHC would not provide the ideal setup to look for those. Instead, high intensity experiments such as neutrino experiments would be valuable tools in probing these “dark sectors.”

## 2 Objectives

The experiment will have a big science reach covering high precision of standard model prediction at low energies through the CE $\nu$ NS interaction and a host of new physics models. The main goals are CE $\nu$ NS detection, BSM interactions, and sterile neutrinos. A general overview of the models are explained below together with the sensitivity analysis to some of the benchmark models.

### 2.1 CE $\nu$ NS detection

In the coherent neutrino-nucleus neutral-current interaction, a neutrino of any flavor scatters off a Si nucleus transferring some energy in the form of a nuclear recoil. The SM cross section  $\sigma$  for this process is [Freedman, 1974].

$$\frac{d\sigma_N^{\text{SM}}}{dE_{\text{rec}}}(E_{\bar{\nu}_e}, E_{\text{rec}}) \simeq \frac{G_F^2}{4\pi} M |f(q)|^2 [Z(4\sin^2\theta_W - 1) + N]^2 \left(1 - \frac{ME_{\text{rec}}}{2E_{\bar{\nu}_e}^2}\right) \quad (1)$$

where  $M$ ,  $N$  and  $Z$  are, respectively, the mass, neutron number and atomic number of the nucleus,  $E_{\bar{\nu}_e}$  and  $E_{\text{rec}}$  are the incident neutrino and the nuclear recoil energy,  $G_F$  is the Fermi coupling constant,  $\theta_W$  is the weak mixing angle, and  $f(q)$  is the nuclear form factor at momentum transfer  $q$ . For  $E_{\bar{\nu}_e} < 50$  MeV, where the momentum transfer ( $q^2$ ) is small enough such that  $q^2 R^2 < 1$ , where  $R$  is the radius of the nucleus [Scholberg, 2006],  $|f(q)| \approx 1$ , within an uncertainty of a few percent [Patton et al., 2012]. At small momentum transfers, the individual nucleon amplitudes are in phase and add coherently, so that the cross section increases by a factor of approximately  $N^2$ .

Although the cross section is enhanced by such coherence, elastic neutrino-nucleus scattering is difficult to observe because of the very small nuclear recoil energies. For silicon atoms the maximum event energy is  $\max(E_{\text{rec}}) = 2E_{\bar{\nu}_e}^2/M$  (approximately 10 keV), showing that this measurement requires very sensitive detectors and a good characterization of the background.

The total cross section  $\sigma_T(E_{\bar{\nu}_e})$  for a mono-energetic neutrino source of energy  $E_{\bar{\nu}_e}$  is given by

$$\sigma_T(E_{\bar{\nu}_e}) = \frac{G_F^2}{4\pi} [Z(4\sin^2\theta_W - 1) + N]^2 E_{\bar{\nu}_e}^2$$

that can be approximated by

$$\sigma_T(E_{\bar{\nu}_e}) \approx 4.22 \times 10^{-45} N^2 E_{\bar{\nu}_e}^2 \quad (2)$$

when  $E_{\bar{\nu}_e}$  is expressed in MeV and  $\sigma_T$  in  $\text{cm}^2$ . The total cross section  $\sigma_T$  for  $^{28}\text{Si}$  ( $N = 14$ ) is shown in blue trace in Fig. 1 as a function of the neutrino energy  $E_{\bar{\nu}_e}$ , showing the small probability for interaction of low energy neutrinos with matter, and its strong dependence on incident energy.

A nuclear power reactor is a high flux source of electron antineutrinos ( $\bar{\nu}_e$ ) with energies up to 12 MeV, approximately. At such energies, the largest probability for interaction with Si atoms is given by the coherent neutrino-nucleus neutral-current interaction. The total cross section  $\sigma_T$  weighted by the  $\bar{\nu}_e$  energy spectrum from a reactor ( $dN_{\bar{\nu}_e}/dE_{\bar{\nu}_e}$ ) is also depicted in Fig. 1 using a red solid line, which is related to the probability of observing a reactor  $\bar{\nu}_e$  of a given energy. The most probable event arises from neutrino energies between 2 and 4 MeV.

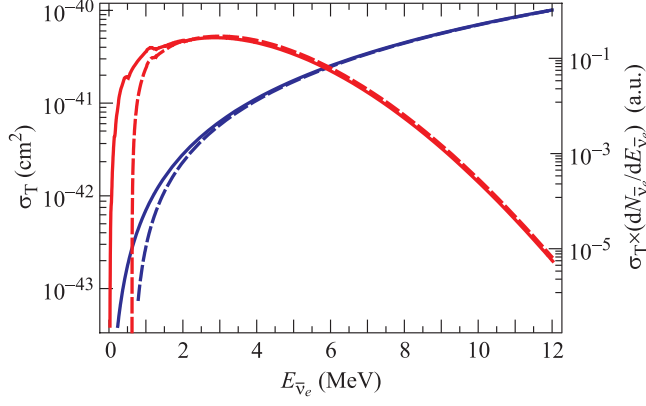


Figure 1: Total neutrino-nucleus coherent cross section  $\sigma_T$  for silicon from Eq. 2 (blue curve, left), and weighted by the reactor antineutrino spectrum (red curve, right). The dashed curves correspond to a threshold energy of 28 eV, approximately  $5\sigma_{RMS}$ .

If the CCD threshold level is considered, the probability of detection is reduced, as depicted by the dashed curves in Fig. 1. In this case, the total cross section is calculated using a threshold of 28 eV, approximately 5 times the minimum RMS noise level ( $\sigma_{RMS}$ ). These results, summarized in Fig. 1, suggest that the low threshold of the detectors is adequate for detecting  $\bar{\nu}_e$  scattering.

## 2.2 BSM scenarios

### 2.2.1 Light mediators

Cross section may be enhanced when we go to low momentum transfer  $q^2 = -2E_R m_{tgt}$ , where  $E_R$  and  $m_{tgt}$  are the recoil and mass of the recoiled target. This is because the propagator in these processes goes like  $g^{\mu\nu}/(q^2 - M_Z^2)$ . The ultra-low thresholds of CCDs may allow to put a strong constraint in such models. Neutrino-electron scattering suffers from smaller cross section but have an even lower  $|q^2|$  due to lighter electron mass. Such extensions of the SM are of interest because there are no constraints from the Large Hadron Collider (LHC) when the mediator mass is below the GeV scale. From the theoretical side, these models have attracted considerable attention because, among other things, they connect to new ideas associated with sub-GeV dark matter in the range of MeV to GeV.

The presence of light force mediators in the neutrino sector would modify scattering cross sections, particularly in low momentum transfer  $q^2 = -2E_r m_{tgt}$ , where  $E_r$  and  $m_{tgt}$  are the energy recoil and mass of the recoiled target. This is because the propagator in these processes goes like  $g^{\mu\nu}/(q^2 - M_Z^2)$ . The ultra-low thresholds of CCDs may allow to put a strong constraint in such models.

More concretely, we will consider light mediator with vector couplings parametrized by the effective Lagrangian

$$\mathcal{L}_{\text{eff}} = g_\nu \bar{\nu}_\alpha \gamma_\mu \nu_\alpha X^\mu + g_q \bar{q} \gamma_\mu q X^\mu + g_\ell \bar{\ell}_\alpha \gamma_\mu \ell_\alpha X^\mu - \frac{M_X^2}{2} X_\mu X^\mu, \quad (3)$$

where a sum over all flavors is implicit and  $X^\mu$  is the new gauge boson with mass  $M_X$ . The elastic neutrino-electron cross sections is given by

$$\begin{aligned} \frac{d\sigma_{\bar{\nu}_e e}}{dE_r} = & \frac{G_F^2 m_e}{2\pi} \left\{ 1 + 4s_W^2 + 8s_W^4 - 2(1 + 2s_W^2) \frac{E_r}{E_\nu} + (1 + 2s_W^2) \left[ (1 + 2s_W^2) \frac{E_r^2}{E_\nu^2} - 2s_W^2 \frac{m_e E_r}{E_\nu^2} \right] \right\} \\ & + \frac{G_F m_e g_\nu g_e}{\sqrt{2}\pi(2E_r m_e + M_X^2)} \left\{ 1 + 4s_W^2 - 2(1 + 2s_W^2) \frac{E_r}{E_\nu} + \left[ (1 + 2s_W^2) \frac{E_r^2}{E_\nu^2} - \left( \frac{1 + 4s_W^2}{2} \right) \frac{m_e E_r}{E_\nu^2} \right] \right\} \\ & + \frac{m_e g_\nu^2 g_e^2}{2\pi(2E_r m_e + M_X^2)^2} \left( 1 - \frac{E_r}{E_\nu} + \frac{E_r^2}{2E_\nu^2} - \frac{m_e E_r}{2E_\nu^2} \right), \end{aligned} \quad (4)$$

where  $G_F$  is the Fermi constant and  $s_W \equiv \sin\theta_W$  is the weak mixing angle. When  $E_r \ll E_\nu$ , this expression can be approximated to

$$\frac{d\sigma_{\bar{\nu}_e e}}{dE_r} \simeq \frac{G_F^2 m_e}{2\pi} (1 + 4s_W^2 + 8s_W^4) + \frac{G_F m_e g_\nu g_e (1 + 4s_W^2)}{\sqrt{2}\pi(2E_r m_e + M_X^2)} + \frac{m_e g_\nu^2 g_e^2}{2\pi(2E_r m_e + M_X^2)^2}. \quad (5)$$

For neutrino-nucleus scattering

$$d\sigma_N/dE_R - d\sigma_N^{\text{SM}}/dE_R = -\frac{G_F m_N Q_v Q'_v (2E_\nu^2 - E_R m_N)}{2\sqrt{2}\pi E_\nu^2 (2E_R m_N + m_{Z'}^2)} + \frac{Q_v'^2 m_N (2E_\nu^2 - E_R m_N)}{4\pi E_\nu^2 (2E_R m_N + m_{Z'}^2)^2} \quad (6)$$

where  $Q_v = N - (1 - 4s_W)Z$  and  $\frac{Q'_v}{g_{\nu,Z'}g_{q,v}} = 3A$ .

For other neutrino-electron and neutrino-nucleus scattering, the cross sections for scalar, pseudoscalar, vector and axial-vector mediators can be found in Table IV of Ref. [Cerdeño et al., 2016] (note that this cross section is independent of the neutrino flavor, as opposed to electron scattering cross section).

Neutrino-electron scattering suffers from smaller cross section but have an even lower  $|q^2|$  due to lighter electron mass.

### 2.2.2 Neutrino magnetic moment

Neutrinos couple to photons via an interaction like  $\mu_\nu \bar{\nu}_L \sigma_{\alpha\beta} \nu_R F^{\alpha\beta}$ . The cross section is enhanced for low recoil, but not as much as in the case of light vector mediators.

### 2.2.3 Dark photons in reactor neutrino experiments

Dark photons could be produced in Compton-like scattering processes [Park, 2017]. This provides a flux of dark photons that could interact in the detector via CEvNS or electron scattering. An excess of events with respect to the standard model expectations, particularly in the low recoil region, would be the signature of this scenario.

### 2.2.4 Sterile neutrinos

Sterile neutrinos are present in several extensions of the standard model, particularly in candidate mechanisms behind neutrino masses, for instance in type I and inverse seesaw scenarios. Here we will focus on light sterile neutrinos invoked to explain the anomalous excesses of events in the LSND and Mini-BooNE [Aguilar-Arevalo et al., 2018] experiments, and the more recent discrepancies with theoretical expectations from short baseline reactor experiments. The short baseline neutrino experiment proposed here would directly probe the reactor anomaly but in a novel way. The experiments that currently test the reactor anomaly use the inverse beta decay process. This proposal would probe the sterile neutrino resolution to the reactor anomaly via neutral current coherent scattering. Neutral current scattering does not distinguish neutrino flavors, and thus is a direct test of the disappearance of standard neutrinos into sterile species.

Nuclear reactors produce  $\bar{\nu}_e$ . The probability of those oscillate to a sterile neutrino at the eV scale is given by, at short baselines,

$$P(\bar{\nu}_e \rightarrow \bar{\nu}_e) \simeq 1 - \sin^2(2\theta_{ee}) \sin^2 \left( 1.27 \frac{\Delta m^2 [\text{eV}^2] L [\text{m}]}{E [\text{MeV}]} \right), \quad (7)$$

where  $\sin^2(2\theta_{ee})$  parametrizes the mixing between electron and sterile flavors,  $\Delta m^2$  is the mass splitting,  $L$  is the baseline and  $E$  is the neutrino energy. The best fit of the reactor anomaly currently points to  $\Delta m^2 = 1.3 \text{ eV}^2$  and  $\sin^2(2\theta_{ee}) = 0.035$ .

In CEvNS with reactor neutrinos, the event rate is dominated by low energy neutrinos with  $E \lesssim \text{MeV}$ . From Eq. (7), considering  $\Delta m^2 = 1.3 \text{ eV}^2$ , one can see that oscillations happen at meter long distances. This is somewhat smaller than commercial nuclear reactor scales. Thus, to properly calculate the reactor neutrino signal at the detector, one needs to integrate over the source position, namely,

$$\langle P(\bar{\nu}_e \rightarrow \bar{\nu}_e) \rangle = \frac{1}{V} \int_{\text{Vol}} d^3 \vec{x}_{\text{src}} P(\bar{\nu}_e \rightarrow \bar{\nu}_e; |\vec{x}_{\text{src}} - \vec{x}_{\text{det}}|), \quad (8)$$

where  $V$  denotes the source volume.

## 2.3 Sensitivity on bench mark models: constraints for light vector mediator

To show the goals and the potential of low energy threshold experiment presented here we evaluate the sensitivity to the light vector mediator explained above using the nuclear and electron recoil channels. And we compare to the best constraints available today.

In Fig. 2 is shown the event spectrum expected in the experiment. The blue curve shows the final observable spectrum after efficiency. This has a strong dependence with energy with two very distinctive signature: the plots grow fast towards low energies and it shows a few notches at specific energies given by the negatives terms in the differential cross section.

In Fig. 3 is shown the expected electron recoils event spectrum in the CCD. It exhibists a strong relationship with energy, specially at low energies. Only very low energy detector can access to this interaction.

To evaluate the sensitivity of the detector we have assumed a simple counting experiment and now spectral information is used at this step. The limit is build using the number of events in the certain energy range to be larger than the background uncertainty with a confidence level of 95%. For nuclear recoils analysis the energy range goes from 15 eV to 100 eV and for the electron from 15 eV to 20 eV. Fig. 4 shows the boundaries of the parametr space covered by the experiment (dashed lines) together with existing best limits. The electron recoil channel allows to explore more than two orders of magnitud in low mass mediators.

### 3 Methodology

#### 3.1 Low threshold detector technologies: Skipper-CCD

With Skipper-CCDs it is possible to achieve an extremely low readout noise of  $0.068e^-_{\text{rms}}/\text{pix}$  [Moroni et al., 2012] [Tiffenberg et al., 2017]. These detectors are developed by the MicroSystem Labs of Lawrence Berkeley National Laboratory and operated at Fermilab. They open an unique opportunity to detect neutrino interactions, that transfer a very small quantity of energy to the Skipper-CCD silicon. A part of the transferred energy is converter in a very small amount of electron-holes pairs that can be easily counted with an Skipper-CCD.

Fully-depleted thick CCDs were developed and fully characterized for the *Dark Energy Camera (DECam)* [Holland et al., 2003][Estrada et al., 2006]. Due to the low readout noise of these CCDs, they are currently applied in the *Dark Matter in CCDs (DMIC)* and in the *Coherent Neutrino Nucleous Interaction Experiment (CONNIE)* [Aguilar-Arevalo et al., 2019]. The only difference of Skipper-CCDs to those CCDs is the output structure, that allows take multiple nondestructive samples of the pixel charge, and then after averaging reduce the readout noise. Because nondestructive readout is achieved without any modification to the CCD fabrication process, this new technology can be directly implemented in existing CCD manufacturing facilities. Skipper-CCDs are p-channel CCDs, fabricated in high resistivity n-type silicon [Holland et al., 2003]. The vertical and horizontal registers have three-phase clocks that are designed for split readout, through the output stage at each quadrant of the sensor. The pixels are squares of  $15 \times 15 \mu\text{m}^2$ . Skipper-CCDs of  $675 \mu\text{m}$  thick has been recently developed for the SENSEI experiment, they can be fully-depleted at a substrate voltage of 40 V.

The sensor is operated in a vacuum chamber and below 140 kelvin to reduce the number of electrons promoted to the conduction band by thermal fluctuations (“dark current”)[Tiffenberg et al., 2017]. The first tests to these devices was done with the Monsoon readout system, originally developed for DECam [Shaw et al., 2010]. To fully benefit from the multiple sampling capabilities of the Skipper-CCD, the noise for each sample must be uncorrelated with the noise of the other samples. For these reason, all correlated noise from the switching mode power supplies (SMPS) was removed, replacing them with linear mode power supplies [Haro et al., 2016b]. Moreover an optimization of the first amplification stages was performed to achieve the minimum noise for one sample [Haro, 2017].

The voltage level of the clock signal are crucial to make the device work. The voltage gradient between the SN, and the summing and output gate was properly adjusted to return all the charge packet from the SN to SW during  $t_2$ . Figure 5 shows that the total amount of the charge packet does not change during the sampling process. The  $V_{\text{ref}}$  voltage and timing of the RG pulse was adjusted to keep the floating gate charged and M1 polarized during the multiple sampling process. The high and low level voltage of the clock phases were adjusted to minimize the generation of spurious charge [Haro et al., 2016a][Haro et al., 2016b].

Fig. 6 shows the single pixel spectrum for different number of samples per pixel, at 200 samples per pixel is possible distinguish peaks of pixels with a discrete number of electrons. As shown in figure 7, for 4000 samples the noise is  $0.068e^-$ , and count the amount of electrons per pixel is possible. At this noise level, the probability that the charge per pixel is misestimated by  $> 0.5e^-$  is  $p \sim 10^{-13}$ . This represents the first accurate single-electron counting on a large-format ( $4126 \times 866$  pixel) silicon detector. Figure 8 shows that the measured noise of the Skipper CCD closely falls with  $\sqrt{N}$ , as was predicted.

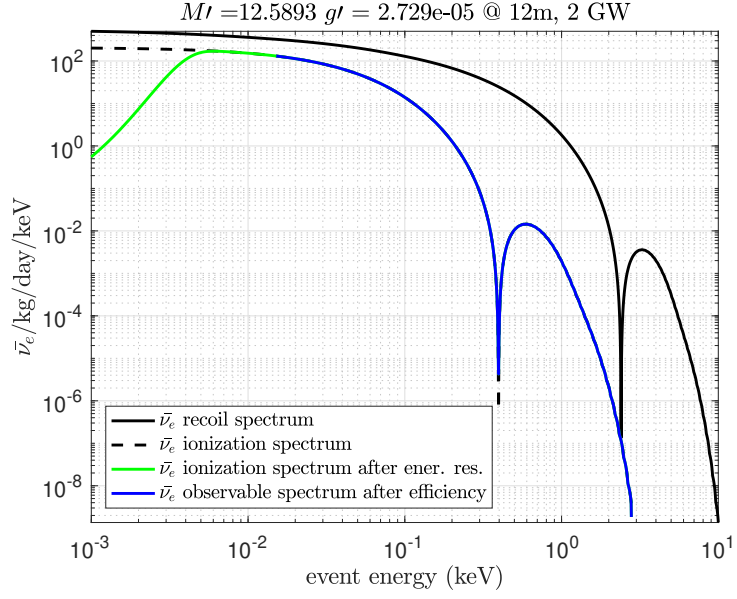


Figure 2: Expected event spectrum from a light vector mediator interacting with the silicon nuclei.

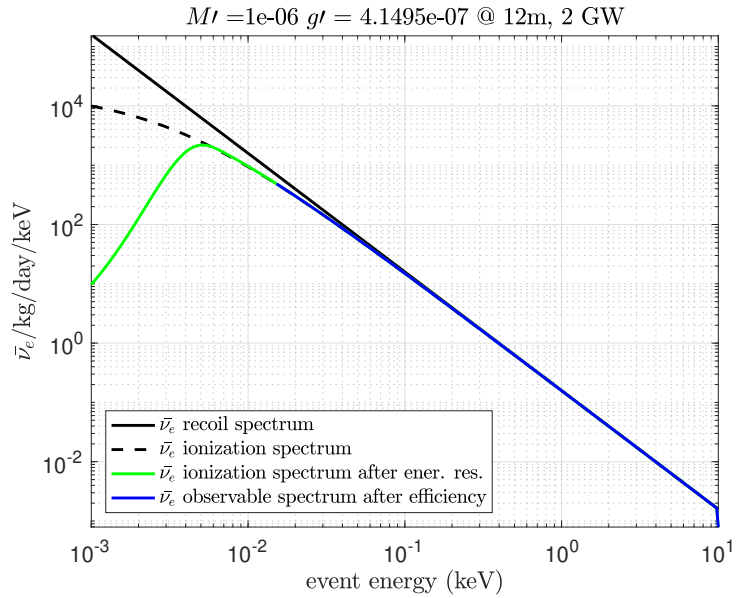


Figure 3: Expected event spectrum from a light vector mediator interacting with electrons.

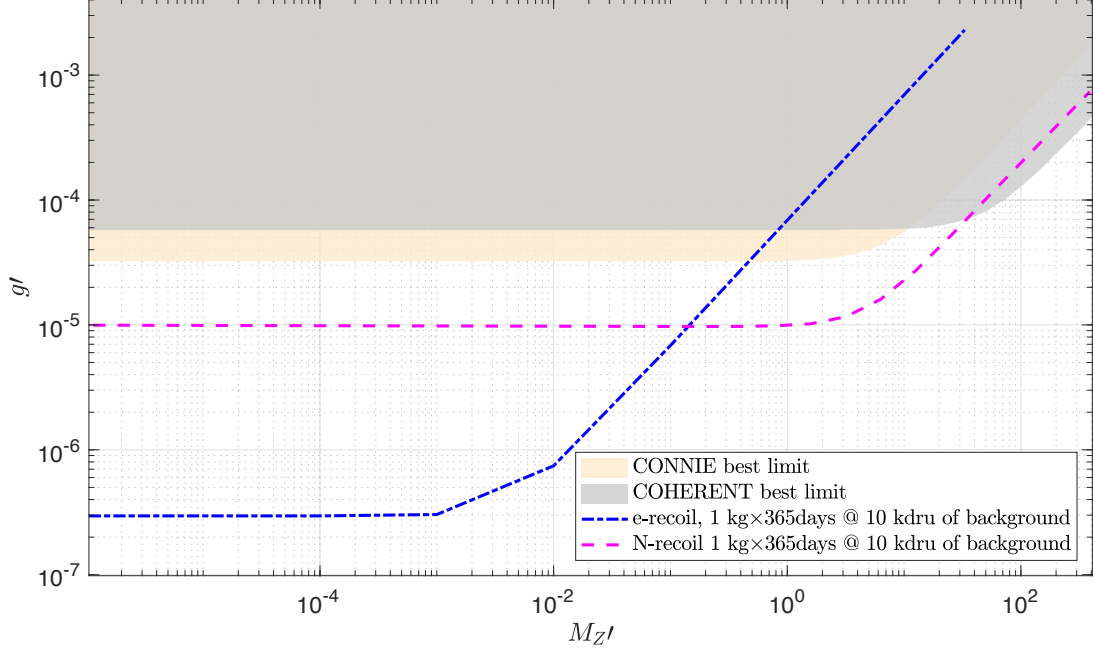


Figure 4: Exclusion boundaries achieved with two different experiment masses. Region above the lines are excluded by the experiment.

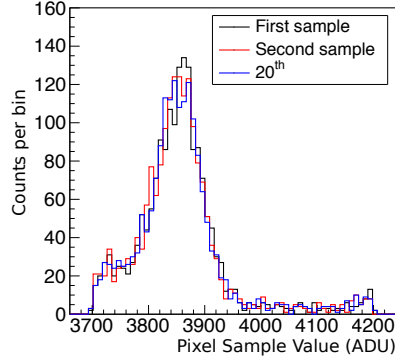


Figure 5: Single pixel spectrum for the first, second and 20<sup>th</sup> sample of all pixels. The peak corresponds to the 5.9 keV X-ray from a <sup>55</sup>Fe source. The peak of the samples are aligned indicating that they have the same charge.

The Skipper CCD studied here has a single-sample readout noise of  $\sigma_1 = 3.55 \text{ e}^-_{\text{rms}}/\text{pixel}$  with a readout time of  $10 \mu\text{s}/\text{pixel}/\text{sample}$ . A readout noise of  $\sigma < 0.1 \text{ e}^-_{\text{rms}}/\text{pixel}$  requires  $\sim 1200$  samples per pixel, corresponding to a readout time of  $12 \text{ ms}/\text{pixel}$ .

### 3.2 Existing CCD readout system (LTA)

As explained in Section 3.1, with the development of fully-depleted Skipper-CCD, it has been possible to experimentally achieve an extremely low readout noise of  $0.068 \text{ e}^-$  [Tiffenberg et al., 2017, Moroni et al., 2012]. Since there was no native controller for Skipper-CCDs, this context has motivated the development of a low-noise electronic controller, which will ease the migration from standard CCDs to Skipper-CCDs. The design of the so called Low-Threshold Acquisition (LTA) system is a joint effort between collaborators from different institutions from Argentina and USA [Haro et al., 2017, Moroni et al., 2019].

The data processing and control of the peripheral components is performed by the Artix-7 FPGA. Bias voltage together with clock generation units create the signals that are necessary to drive the CCD. The board has four video channels, built with 18-bit, 15 MSPS analog-to-digital converters tightly coupled with low-noise differential operational amplifiers to digitize the analog video signals. Output samples of the converters are fed into the FPGA to perform digital filtering and image reconstruction.



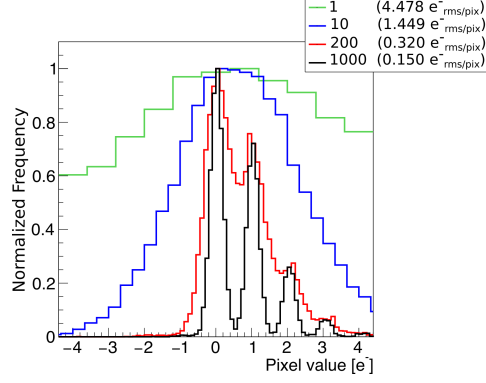


Figure 6: Single pixel spectrum of a image region for different amount of samples per pixel. The pixel value was calibrated using the system gain obtained from a exposure of the detector to a  $^{55}\text{Fe}$  source. The spectrum is shown after averaging different amount of samples per pixel. For 1000 samples individual electron counting per pixel is possible.

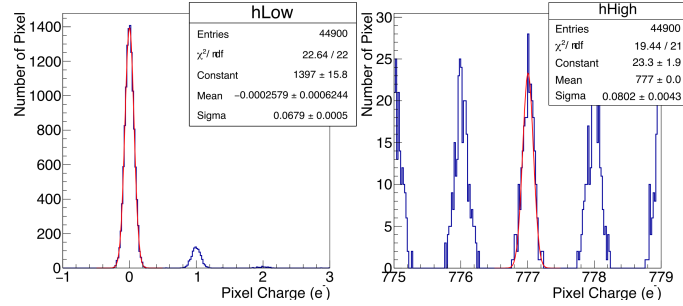


Figure 7: Single-electron charge resolution using a Skipper CCD with 4000 samples per pixel (bin width of  $0.03\text{ e}^-$ ). The measured charge per pixel is shown for low (main) and high (inset) illumination levels. Integer electron peaks can be distinctly resolved in both regimes contemporaneously. The  $0\text{ e}^-$  peak has RMS noise of  $0.068\text{ e}^-_{\text{rms}}/\text{pixel}$  while the  $777\text{ e}^-$  peak has  $0.086\text{ e}^-_{\text{rms}}/\text{pixel}$ , demonstrating single-electron sensitivity over a large dynamical range. The Gaussian fits have  $\chi^2 = 22.6/22$  and  $\chi^2 = 19.5/21$ , respectively.

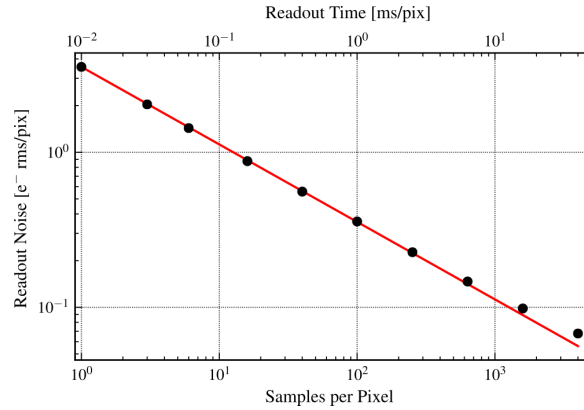


Figure 8: Readout noise as a function of the number of nondestructive readout samples per pixel for the Skipper CCD. Black points show the rms of the empty-pixel distribution as a function of the number of averaged samples. The red line is the theoretical expectation assuming independent, uncorrelated samples.

Output data is sent to a personal computer through the Ethernet port. The user interacts with the board through a single Ethernet port, which allows sending and receiving commands as well as data. Serial interface is reserved for debugging purposes.

The readout board incorporates a low-speed analog-to-digital converter together with analog multi-

plexers, that allow monitoring all voltages and clock signals. This sub-system is called telemetry, and the data collected can be also transferred using the Ethernet port. In this way the user can monitor the internal variables of the system remotely, without the need of adding extra hardware or complex communication mechanisms. A detailed description of the design and test of the front-end electronics can be found in [Haro et al., 2017, Moroni et al., 2019].

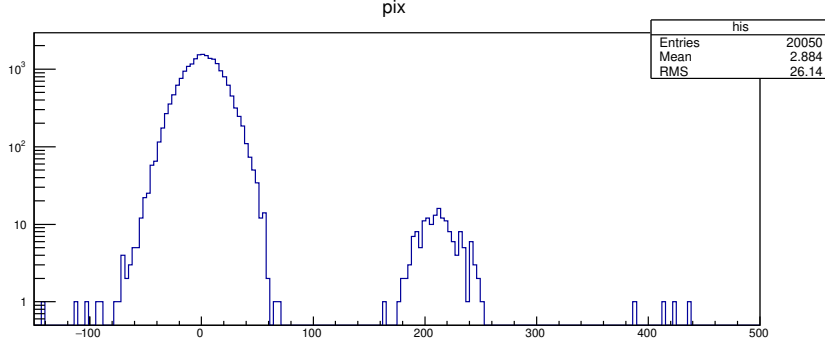


Figure 9: Histogram computed for the pixels of a Skipper-CCD image acquired with the LTA electronics. x-axis: analog to digital converter units (ADU); y-axis: amount of pixels.

The skipper readout capability and the noise performance of the LTA readout system was evaluated. An Skipper-CCD image reading out 2000 times the charge of each pixel was taken from a fraction of the CCD of size  $50 \times 401$  pixels. Figure 9 shows a histogram (in log scale) of the pixels array after averaging the 2000 readouts of each pixel. Two peaks with Gaussian distribution that correspond to empty pixels (highest peak) and pixels with single electrons events (lowest peak). A noise of  $\approx 0.076e^-$  was obtained, which showed the capability of the electronics of achieving sub electron noise. Figure 10 shows the experimental setup used for the testing of the LTA board.

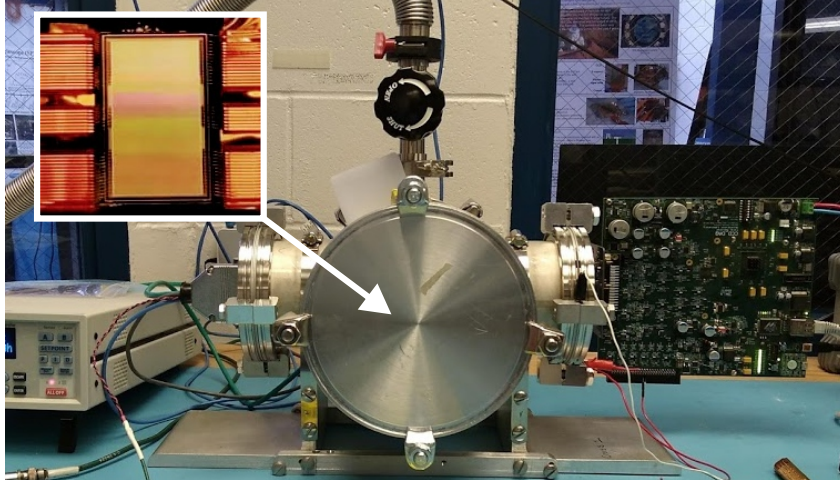


Figure 10: Photograph of the LTA electronics on the experimental setup. Images includes dewar, readout electronics and the Skipper sensor.

An other advantage of the LTA electronics is that, due to the digital sampling of the video signal, it is possible to compute signal processing algorithms for noise reduction. In this line, optimal filters to compute the pixel values minimizing the noise variance have been studied [Simbeni et al., 2019]. Also due to the flexibility in the programming of the sequencer, alternative readout techniques to reduce correlated noise between channels were developed [Fernandez Moroni G., 2020]. This technique could be useful for new experiments using many CCD detectors with hundreds or thousands of channels where common noise due to long wiring and distributed signal processing can results in higher correlated noise.

### 3.3 State-of-the-art of the Ionization Efficiency for nuclear recoils in silicon

Nuclear recoil efficiency is important to evaluate the observable ionization from nuclear recoil interactions. Figure 11 shows the current status of the Ionization Efficiency measurements in silicon. The plot summarizes previous experimental measurements, Lindhard theoretical calculation and the contributions of the CCD detector community, highlighted in red and green. The overall trend of  $\varepsilon$  is well described by Lindhard theory above  $\approx 4$  keV<sub>NR</sub> of recoil energy. Below this energy, the presented measurements show, for the first time, a deviation of Lindhard theory, in which the ionization efficiency drops faster than the model.

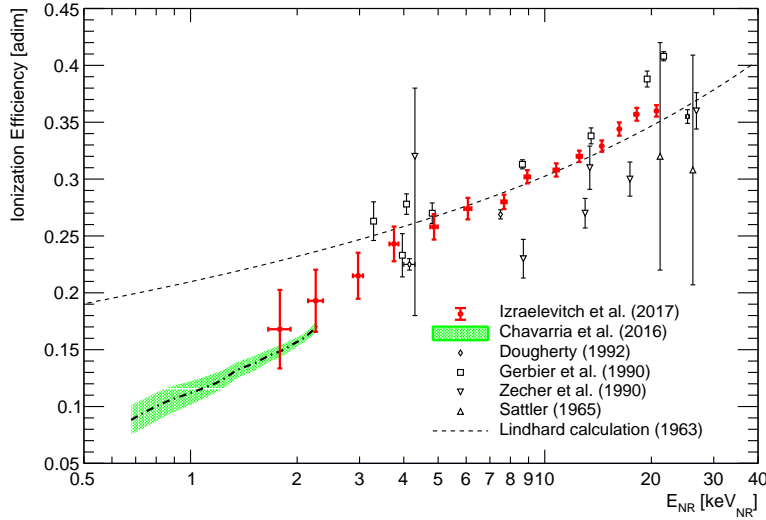


Figure 11: Ionization efficiency (ratio between the energy released via ionization and the nuclear recoil energy) as a function of the nuclear recoil energy. The green-shaded area is the results of the photon-neutron source experiment [Chavarria et al., 2016] and the red-solid data points are the results of the accelerator-based experiment [Izraelevitch et al., 2017]. Data points from previous experiments: upward-pointing empty triangles from Sattler [Sattler, 1965], downward-pointing empty triangles from Zecher *et al.* [Zecher et al., 1990], empty squares from Gerbier *et al.* [Gerbier et al., 1990], empty diamonds from Dougherty [Dougherty, 1992]. The dashed curve is Lindhard prediction for silicon [Lindhard et al., 1963].

### 3.4 Background inside reactor buildings

For reactor neutrino experiments such as the one we are proposing here, using very low energy threshold detectors, it is crucial to control the background. For this sake, we need to understand the different background sources and reduce them as much as possible. In particular, it is mandatory to have a good understanding of the neutron-induced background since neutron recoil signals can mimic the interaction of a neutrino in the detector. This becomes a key issue as we are planning to install the detector at a distance as close as possible to the reactor core. Recently, the CONUS collaboration published a detailed study of the neutron induced background for their experiment and demonstrated that it is possible to reduced significantly this background contribution [Hakenmüller et al., 2019]. The CONUS experiment consists in high-purity germanium (HPGe) detectors installed at  $\sim 17$  m from the core of a commercial 4 GW reactor in Germany. For this kind of experiment we can divide the neutron induced background into two groups: (i) related to the reactor activity, mainly neutrons coming from the core and  $\gamma$ -radiation from neutron-induced isotopes decaying along the primary coolant of the pressurized water reactor; (ii) independent from the reactor operation, such as neutrons induced by cosmogenic muons interacting in the reactor building and in the experiment shield and some ( $\alpha$ ,n) reactions from natural radioactivity in the surrounding concrete walls and basements. This second group is always present independently of the reactor activity and should be reduced as much as possible in order to be able to statistically measure the CEvNS.

In reference [Hakenmüller et al., 2019] the CONUS collaboration shows that using a passive shield

made with different layers of lead (Pb, 25 cm total) intercalated with normal and borated polyethylene (2 layers of 10 cm each at 3% equivalent of natural B). The Pb installed in all directions is employed to suppress external  $\gamma$ -radiation while the polyethylene (PE) is inserted to moderate and capture neutrons from outside as well as neutrons created by muons in the Pb layers of the shield. With this shield configuration the CONUS collaboration has shown that there is no difference in the neutron signal with the reactor on and off. This shows that it is possible to operate a neutrino detector inside the contention sphere, without contamination of the signal by neutrons.

In addition to the passive shield, CONUS has an active muon veto system made of organic plastic scintillator plates (of 5.2 cm thickness) equipped with photomultiplier tubes. The muon veto is very important to reduce the cosmogenic neutrons induced by muons. It is possible to use such a veto in CONUS as the HPGe detectors have a good time resolution. However, it is not possible to have anything like that for the Skipper-CCDs we are proposing to use, as they are exposed for a long period of time, such that they don't have temporal resolution for when the particle interactions occur.

The CONNIE experiment [Aguilar-Arevalo et al., 2019], located at 30 m from a reactor core at Angra 2 in Brazil, is placed outside the reactor contention sphere in a container. CONNIE uses a passive shield made by 15 cm of lead and two layers of high density PE of 30 cm each. The observed background, mainly due to the cosmogenic contribution is 10 kdru. This value is used for all the estimations calculated in the present paper as an upper limit. With the detector placed closer to the reactor core, inside the reactor building and using a passive shield we expect to reduce this background by a factor of 2-10.

For the present proposal we are planning to use all the expertise coming from the different local groups to measure and characterize the background as much as possible. For this sake, we plan to install at the experiment site different neutron detectors and muon telescopes. First of all, we need to demonstrate that we do not see the reactor, i.e., we have the same background levels when the reactor is on and off. Once we reach this stage, we will focus on the cosmogenic background. Following this strategy we will ensure the experiment will have the capability to see the CEvNS interaction.

### 3.5 Reactor facilities in Argentina

Argentina has three power reactors whose main characteristics are summarized in Table 3.5. There are also several research reactors, being the most larger (facilities with a power equal or above 1 MW) briefly described in Tables 3.5.

Table 3.5 also includes RA10, a reactor for research a radionuclides production under construction.

	Research reactor		
Name	RA6	RA3	RA10
Power (MWth)	1	10	30
Type	Pool	Pool	Pool
Fuel	$^{235}\text{UO}_2$ (20%)	$^{235}\text{UO}_2$ (20%)	LEU*
Reactor ON/Reactor OFF	1	1	5
Location	Bs. As.	Ezeiza	Ezeiza
Status	Operational	Operational	Under Construction
Operator	CNEA	CNEA	CNEA

Table 1: Main characteristics of research reactors with power above 1 MW in Argentina. \*Low enriched uranium.

	Power reactor		
Name	Atucha 1	Atucha 2	Embalse
Power (MWth)	1179	2161	2015
Type	PHWR	PHWR	PHWR
Vessels diameters (mm)	6200	8340	$\approx 8000$
Fuel	ULE (0.85%)	Natural UO2	Natural UO2
Reactor ON/Reactor OFF	12	12	13
Location	Lima	Lima	Embalse Rio Tercero
Status	Operational	Operational	Operational
Operator	NASA	NASA	NASA

Table 2: Main characteristics of power reactors in Argentina.

Based on this information we calculate the relation ship between the distance from a detector to the center of the reactor core and the parameter mass by time for a given sensitivity. Figure 12 presents the result obtained for a 95% of confidence level in measuring the CE $\nu$ Ns interaction. These calculation were performed under the point-like reactor approximation, which will be discussed in the next subsection. Taking into account the ratio between Reactor ON and Reactor OFF, also indicated in Tables 3.5 and 3.5, we show in figure 13 how the significance increases as exposure time of the experiment goes by. Once again, we used the mass by time as the figure of merit to depict the behavior of this quantity.

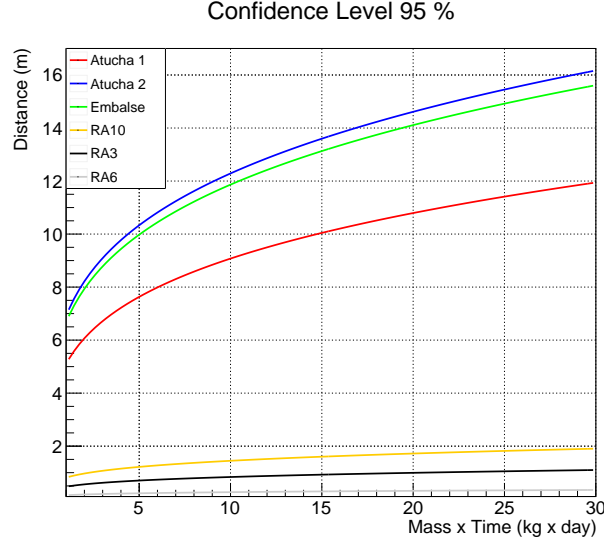


Figure 12: Curves of 95% of confidence level of measuring the CE $\nu$ Ns interaction for different reactors in Argentina. These curves allow to know the relationship between distance and Mass by Time of exposure for a given confidence level.

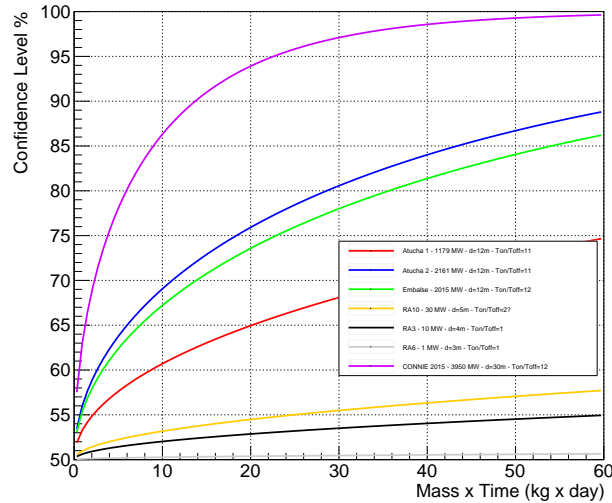


Figure 13: Confidence level of measuring the CE $\nu$ Ns interaction as a function of the Mass by Time of exposure for different reactors in Argentina. For each reactor the core to reactor face distance was considered for the experiment.

According to figures 12 and 13, Atucha 2 seems to be the reactor that offers the best conditions for a neutrino experiment, since at 12 m from the reactor core center, with a detector of 1 kg, 10 days is enough to reach a 95% of confidence level in the CE $\nu$ Ns detection. Atucha 2 is a pressurized heavy water

reactor of german design (Siemens). It has a thermal power of 2161 MW (nominal), 451 fuel elements, each one with an active length equal to 5.3 m and a diameter of nearly 10 cm (they have a cylindrical shape). The fuel elements are vertically allocated inside a pressure vessel (14 meters high and 8.44 meters wide i.e., diameter) in a triangular grid, the distance between fuel elements centers is 27.2 cm

## References

- [Aguilar-Arevalo et al., 2019] Aguilar-Arevalo, A., Bertou, X., Bonifazi, C., Cancelo, G., Castañeda, A., Cervantes Vergara, B., Chavez, C., D’Olivo, J. C., dos Anjos, J. a. C., Estrada, J., Fernandes Neto, A. R., Fernandez Moroni, G., Foguel, A., Ford, R., Gonzalez Cuevas, J., Hernández, P., Hernandez, S., Izraelevitch, F., Kavner, A. R., Kilminster, B., Kuk, K., Lima, H. P., Makler, M., Molina, J., Mota, P., Nasteva, I., Paolini, E. E., Romero, C., Sarkis, Y., Sofo Haro, M., Souza, I. a. M. S., Tiffenberg, J., and Wagner, S. (2019). Exploring low-energy neutrino physics with the coherent neutrino nucleus interaction experiment. *Phys. Rev. D*, 100:092005.
- [Aguilar-Arevalo et al., 2018] Aguilar-Arevalo, A., Brown, B., Bugel, L., Cheng, G., Conrad, J., Cooper, R., Dharmapalan, R., Diaz, A., Djurcic, Z., Finley, D., and et al. (2018). Significant excess of electron-like events in the minibooone short-baseline neutrino experiment. *Physical Review Letters*, 121(22).
- [Cerdeño et al., 2016] Cerdeño, D. G., Fairbairn, M., Jubb, T., Machado, P. A. N., Vincent, A. C., and Boehm, C. (2016). Physics from solar neutrinos in dark matter direct detection experiments. *Journal of High Energy Physics*, 2016(5).
- [Chavarria et al., 2016] Chavarria, A., Collar, J., Peña, J., Privitera, P., Robinson, A., Scholz, B., Sengul, C., Zhou, J., Estrada, J., Izraelevitch, F., et al. (2016). Measurement of the ionization produced by sub-keV silicon nuclear recoils in a ccd dark matter detector. *Physical Review D*, 94(8):082007.
- [Dougherty, 1992] Dougherty, B. L. (1992). Measurements of ionization produced in silicon crystals by low-energy silicon atoms. *Physical Review A*, 45(3):2104.
- [Estrada et al., 2006] Estrada, J., Abbott, T., Angstadt, B., Buckley-Geer, L., Brown, M., Campa, J., Cardiel, L., Cease, H., Flaughner, B., Dawson, K., et al. (2006). Ccd testing and characterization for dark energy survey. In *Ground-based and Airborne Instrumentation for Astronomy*, volume 6269, page 62693K. International Society for Optics and Photonics.
- [Fernandez Moroni G., 2020] Fernandez Moroni G., Chierchie F., e. a. (2020). Interleaved Readout of Charge Coupled Devices (CCDs) for Correlated Noise Reduction. *IEEE Transactions* (under review).
- [Freedman, 1974] Freedman, D. Z. (1974). Coherent effects of a weak neutral current. *Phys. Rev. D*, 9:1389–1392.
- [Gerbier et al., 1990] Gerbier, G., Lesquoy, E., Rich, J., Spiro, M., Tao, C., Yvon, D., Zylberajch, S., Delbourgo, P., Haouat, G., Humeau, C., et al. (1990). Measurement of the ionization of slow silicon nuclei in silicon for the calibration of a silicon dark-matter detector. *Physical Review D*, 42(9):3211.
- [Hakenmüller et al., 2019] Hakenmüller, J., Buck, C., Fülber, K., Heusser, G., Klages, T., Lindner, M., Lücke, A., Maneschg, W., Reginatto, M., Rink, T., Schierhuber, T., Solasse, D., Strecker, H., Wink, R., Zbořil, M., and Zimbal, A. (2019). Neutron-induced background in the conus experiment. *The European Physical Journal C*, 79(8):699.
- [Haro et al., 2016a] Haro, M., Moroni, G., Tiffenberg, J., Cancelo, G., Estrada, J., Bertou, X., and Paolini, E. (2016a). Taking the ccds to the ultimate performance for low threshold experiments. Technical report, Fermi National Accelerator Lab.(FNAL), Batavia, IL (United States).
- [Haro, 2017] Haro, M. S. (2017). Single electron per pixel counting with fully depleted charge coupled devices. In *2017 IEEE Nuclear Science Symposium and Medical Imaging Conference (NSS/MIC)*, pages 1–3. IEEE.
- [Haro et al., 2016b] Haro, M. S., Cancelo, G., Moroni, G. F., Bertou, X., Tiffenberg, J., Paolini, E., and Estrada, J. (2016b). Measurement of the read-out noise of fully depleted thick ccds. In *2016 Argentine Conference of Micro-Nanoelectronics, Technology and Applications (CAMTA)*, pages 11–16. IEEE.

- [Haro et al., 2017] Haro, M. S., Soto, A., Moroni, G. F., Chierchie, F., Stefanazzi, L., Chavez, R., Castaneda, A., Hernandez, K., Zmuda, T., Wilser, N., Paolini, E., Oliva, A., and Cancelo, G. (2017). A low noise digital readout system for scientific charge coupled devices. In 2017 XVII Workshop on Information Processing and Control (RPIC), pages 1–5.
- [Holland et al., 2003] Holland, S. E., Groom, D. E., Palaio, N. P., Stover, R. J., and Wei, M. (2003). Fully depleted, back-illuminated charge-coupled devices fabricated on high-resistivity silicon. Electron Devices, IEEE Transactions on, 50(1):225–238. doi: 10.1109/TED.2002.806476.
- [Izraelevitch et al., 2017] Izraelevitch, F., Amidei, D., Aprahamian, A., Arcos-Olalla, R., Cancelo, G., Casarella, C., Chavarria, A., Collon, P., Estrada, J., Moroni, G. F., et al. (2017). A measurement of the ionization efficiency of nuclear recoils in silicon. Journal of Instrumentation, 12(06):P06014.
- [Lindhard et al., 1963] Lindhard, J., Scharff, M., and Schiott, H. (1963). Mat. Fys. Medd. Dan. Vid. Selsk., 33(10).
- [Moroni et al., 2019] Moroni, G. F., Chierchie, F., Haro, M. S., Stefanazzi, L., Soto, A., Paolini, E. E., Cancelo, G., Treptow, K., Wilser, N., Zmuda, T., Estrada, J., and Tiffenberg, J. (2019). Low Threshold Acquisition Controller for Skipper Charge Coupled Devices. In 2019 Argentine Conference on Electronics (CAE), pages 86–91.
- [Moroni et al., 2012] Moroni, G. F., Estrada, J., Cancelo, G., Holland, S. E., Paolini, E. E., and Diehl, H. T. (2012). Sub-electron readout noise in a Skipper CCD fabricated on high resistivity silicon. Experimental Astronomy, 34(1):43–64.
- [Park, 2017] Park, H. K. (2017). Detecting dark photons with reactor neutrino experiments. Phys. Rev. Lett., 119:081801.
- [Patton et al., 2012] Patton, K., Engel, J., McLaughlin, G. C., and Schunck, N. (2012). Neutrino-nucleus coherent scattering as a probe of neutron density distributions. Phys. Rev. C, 86:024612.
- [Sattler, 1965] Sattler, A. (1965). Ionization produced by energetic silicon atoms within a silicon lattice. Physical review, 138(6A):A1815.
- [Scholberg, 2006] Scholberg, K. (2006). Prospects for measuring coherent neutrino-nucleus elastic scattering at a stopped-pion neutrino source. Phys. Rev. D, 73:033005.
- [Shaw et al., 2010] Shaw, T., Ballester, O., Cardiel-Sas, L., Castilla, J., Chappa, S., De Vicente, J., Holm, S., Huffman, D., Kozlovsky, M., Martínez, G., et al. (2010). System architecture of the Dark Energy Survey Camera readout electronics. In SPIE Astronomical Telescopes+ Instrumentation, pages 77353G–77353G. International Society for Optics and Photonics.
- [Simbeni et al., 2019] Simbeni, P. Q., Moroni, G. F., Chierchie, F., Paolini, E., Haro, M. S., Soto, A., Stefanazzi, L., Cancelo, G., and Estrada, J. (2019). Optimal Filter Design Considering Charge Transfer Characteristics for CCD Readout. In 2019 Argentine Conference on Electronics (CAE), pages 41–46.
- [Tiffenberg et al., 2017] Tiffenberg, J., Sofo-Haro, M., Drlica-Wagner, A., Essig, R., Guardincerri, Y., Holland, S., Volansky, T., and Yu, T.-T. (2017). Single-Electron and Single-Photon Sensitivity with a Silicon Skipper CCD. Phys. Rev. Lett., 119:131802.
- [Zecher et al., 1990] Zecher, P., Wang, D., Rapaport, J., Martoff, C., and Young, B. (1990). Energy deposition of energetic silicon atoms within a silicon lattice. Physical Review A, 41(7):4058.